Computational Modeling of the CH-47 Helicopter in Hover

Arsenio C.B. Dimanlig
ELORET/NASA-Ames Research Center, Moffett Field, CA
adimanlig@mail.arc.nasa.gov

Edward T. Meadowcroft
Boeing Integrated Defense Systems – Rotorcraft Systems, Philadelphia, PA
ted.meadowcroft@boeing.com

Roger Strawn and Mark Potsdam
US Army Research, Development, and Engineering Command, Aeroflightdynamics Directorate, Moffett Field, CA
{rstrawn, mpotsdam}@mail.arc.nasa.gov

Abstract

This paper describes installed rotor performance computations for the CH-47 Chinook tandem-rotor helicopter. The computations were performed with a Reynolds-Averaged Navier-Stokes flow solver using overset structured grids to resolve the flow around the rotors, the fuselage, and the resulting rotor wake system. The calculations model all six rotor blades discretely while resolving the rotor motions relative to the fuselage in a time-accurate manner. The computational performance predictions are compared to Boeing flight test data and show good agreement with the experimental measurements. In addition, the computational results provide a wealth of data on the interactions between the rotor wake system and the fuselage that can't be easily obtained in any other way.

1. Introduction

Although computational fluid dynamics (CFD) methods are often used to model complete fixed-wing aircraft, CFD simulations for complete helicopters are relatively rare. The helicopter problem is much more complex than its fixed-wing counterpart due to three factors: 1) relative motion between the discrete rotors and the fuselage, 2) the requirement to iteratively trim the aerodynamic and dynamic forces, and 3) the importance of high-fidelity resolution of the rotor wake system.

Despite this high complexity, there is a high payoff for full-vehicle helicopter modeling because the details of the rotor-rotor and/or rotor-fuselage interactions are typically very important in determining the overall performance of the aircraft. Although computationally intensive, these full-vehicle discrete-rotor CFD simulations provide a wealth of flowfield details that can't be easily obtained in any other way.

One of the first complete-vehicle discrete-blade CFD simulations was performed by Potsdam and Strawn[1] for the V-22 tilt-rotor in hover. This computation modeled two unsteady rotors over the V-22 fuselage using an overset grid system with about 50 million grid points. This paper used basically the same overset-grid computational approach as is used in the current CH-47 simulations. More recent full-vehicle discrete-rotor simulations have been shown by Khier, et al.[2], and Pahlke et al.[3], also using overset structured-grid methods.

2. Boeing CH-47 Helicopter

The CH-47D/F Chinook is a multi-mission, medium/heavy-lift transport helicopter. Its primary mission is to move troops, artillery, ammunition, fuel, water, barrier materials, supplies and equipment on the battlefield. In various alternate configurations, its additional missions include medical evacuation, disaster relief, search and rescue, aircraft recovery, fire fighting, parachute drops, heavy construction and civil development.

Objectives of the collaborative CFD effort are to develop an overset structured grid model of the fuselage and tandem rotors. The rotors can be modeled as momentum source disks or with discrete moving blades. The rotor blade material can be assumed rigid with prescribed control inputs or the model can be coupled with a suitable comprehensive structural dynamics model.

0-7695-3088-5/07 $25.00 © 2007 IEEE

3. Description of Test Data

During 1983, Boeing conducted tethered hover flight tests of the CH-47D at St. Paul, MN; Edwards AFB, CA; Bishop, CA; and Coyote Flats, CA. Testing included hover performance, compressibility power trends, and ground effects. The testing out of ground effect was conducted at an aircraft wheel height of 150 feet. Testing was conducted in ambient winds less than 5 knots.

Torque was measured by rotor shaft torque sensors and engine torque data. Total system thrust was measured with a calibrated flexible load cell. The download was estimated using an empirical method as described in Stepniewski and Keys[4].

The experimental and computational comparisons in the following sections will present non-dimensional and scaled experimental data in ways that give meaningful comparisons with computational results without showing the absolute performance numbers for the CH-47.

4. Computational Method

The computational model for this work uses the OVERFLOW-2 Reynolds-Averaged Navier-Stokes computational fluid dynamics code[5]. The OVERFLOW-2 code includes all the major modifications made in OVERFLOW-2[6] for time-dependent, rigid body motion of components. In particular, the OVERFLOW-2 code models the independent relative motion between component parts, which is often required for complex rotorcraft configurations.

OVERFLOW-2 uses a system of structured overset grids to discretize the computational domain. Curvilinear grids surround the rotors and the fuselage (near-body grids) and a system of uniform Cartesian grids covers the remaining regions away from the solid surfaces (off-body grids). These off-body grids are primarily used to capture the discrete vortices in the rotor wake system.

The off-body grids are clustered in several levels with grid spacing increased by a factor of two at each level until reaching the outer boundary of the computational domain. Information between the various grid systems (domain connectivity) is exchanged through interpolations at the inter-grid boundaries. Relative grid motion necessitates recalculation of the domain connectivity at each time step as the near-body grids move through the stationary off-body grids.

Central spatial differencing is used for the convective terms and the time-accurate simulations make use of a dual-time stepping scheme to ensure accuracy and numerical stability. Time steps are typically 0.25 degrees of rotor azimuth. To better capture the tip vortices in the rotor wake system, a fourth-order spatial-differencing scheme is applied to the convective terms in the background meshes.

Initial computations used a matrix dissipation scheme to improve numerical accuracy. However the flowfield solutions with matrix dissipation exhibited instabilities in the far-field wake system. As a result, the solutions in this paper wound up employing a more conventional fourth-order scalar dissipation scheme which is more diffusive than its matrix dissipation counterpart. However, the scalar dissipation results didn't show any far-field instabilities in the wake system grids.

The effects of surface boundary-layer turbulence are modeled using the Spalart-Allmaras one-equation turbulence model. For the off-body grids, the viscous terms are not included since the grid-related dissipation is already much larger than any viscous dissipation that might be present in the solution.

5. CH-47 Grid System and Modeling Details

The computational models for the rotors and fuselage were derived from full- configuration CAD data provided by Boeing. Figure 1 shows the overset surface grid for the helicopter fuselage. While basically true to the CAD model, this geometry was simplified to expedite the grid generation process. This included modeling a fairing on each of the external openings such as the main rotor hub well. Also, certain fuselage components were excluded in the grid system since their influence on vehicle hover performance is minimal. The excluded fuselage details include, the landing gears and gear wells, antennae, engine nacelles and other protrusions.

There are 49 interconnected body-fitted grids that make up the fuselage. Each blade has 3 body-fitted O-mesh grids for a total of 18 for the entire rotor system. Figure 2 shows the surface grid system for one of these rotor blades.

The rest of the off-body grid components are comprised of uniform Cartesian grids generated by the flow solver. The grid spacing on the finest Cartesian grids is equal to 0.06 blade chord lengths in the regions surrounding the rotor and fuselage. The grid spacing in these off-body grids increases monotonically with distance from the fuselage to the far-field boundaries where the computational domain ends at about seven fuselage lengths from the body in all directions. The near-body and off-body meshes have a total of 166 interconnected grids in the entire flow field. Approximately 78 million grid points were used for the complete grid system.

For the installed-rotor configuration on the IBM P5, 1,440 time steps can be run on 256 processors in about 12.5 hours. These installed rotor cases were run until the

load histories for the fuselage and both rotor blades showed steady cyclical behavior.

Ideally, the computed thrust and moment values from each rotor should be iteratively trimmed about the vehicle center of gravity in order to match up with the flight test force and moment data. In addition, the CFD model should be trimmed to match rotor hub moments. Finally, the computations should include the elastic deflections of the rotor blades, which may have a significant influence on the rotor thrust and power.

Unfortunately the addition of aeroelastic coupling and iterative trim for these full-vehicle CH-47 calculations only adds to what is already a very large computational cost. For this reason, we decided not to include these factors for our initial tests of the CFD model. As a result, the CFD model and the actual aircraft differ in their treatment of structural dynamics and trim.

On the actual aircraft, the pilot controls total thrust, differential thrust, cyclic for lateral motion, and cyclic to yaw the aircraft (differential tilting of thrust vectors to yaw). For hover, the rotors are trimmed to differential thrust to balance pitch moment. The forward and aft rotor thrusts typically differ by about 8%, which can change in order to account for the distribution of payload around the aircraft center of gravity. This difference in thrust (and therefore torque) between the two rotors produces a yawing moment which is trimmed with differential lateral cyclic. Lateral cyclic also trims the fuselage side force due to sidewash from the rotor wake.

In addition, the rotor overlap region produces thrust and power loads with high frequency content. The cyclic pitch variations used to trim these forces is small. The aerodynamic forces on the rotor, the blade mass and material properties, and the control settings establish rotor flapping and blade elastic deformations.

On the installed-rotor CFD model, all rotor and fuselage control settings and attitudes were held fixed. The settings were prescribed by Boeing, based on existing analyses. These settings included the rotor collective, rotor tip path planes, coning angles, and fuselage attitude. The rotor blades were assumed to be rigid and a decision was made to set front and rear rotor collectives to the same value, rather than to try to trim to prescribed, non-equal thrust targets.

With these control settings, the computational results for the three cases show that the integrated forces on the front and rear rotors are virtually the same, with thrust and torque differences of less than 0.5%. More sophisticated control of the full-vehicle trim requires iterative coupling with a structural-dynamics model for the rotor and fuselage.

6. Installed Rotor Results

The installed rotor computations were run at rotor collective angles of 8°, 10°, and 12°. The fore and aft rotors used the identical collective settings in each of the three computations. The rotor tip path planes were specified by Boeing. These tip path planes are set so that they overlap for maximum hover efficiency.

The initial hover calculations at the lowest thrust level were started from scratch and run for approximately 15 rotor revolutions until the rotor forces and wake system were periodic. Subsequent hover calculations at higher thrust levels were restarted from previous solutions and run for approximately seven additional rotor revolutions until both the rotor and fuselage forces became periodic. This periodicity in rotor thrust is shown in Figure 3, which shows the thrust for each rotor as a function of the number of rotor revolutions.

Figure 3 shows that the thrust on each rotor is very consistent and periodic over the last three rotor revolutions. The thrust on the front and rear rotors is 60° out of phase, as expected, but the magnitudes of the thrust on each blade are the same, indicating an equal sharing of thrust between the front and rear rotors.

Figure 4 shows the time-accurate thrust values for the entire vehicle. This thrust oscillates as each rotor passes over the fuselage, causing a periodic loss of thrust due to the fuselage download. Although the thrust values in Figure 4 are reasonably steady over the last seven rotor revolutions, they don't quite show the same repeatability that is seen in Figure 3 for the individual rotors.

This low-frequency unsteadiness is caused by unsteady vortex shedding from the underside of the CH-47 fuselage. Since the magnitudes of these thrust oscillations are small and the frequency low, no further attempts were made to continue the computations beyond this point. Detailed characterization of this low-frequency unsteadiness would have required substantially longer computational run times.

Figure 5 shows the computed pressures contours on the CH-47 fuselage plus the computed wake geometry. The computed rotor wake vortices are represented by iso-surfaces of the second invariant, **Q**, of the velocity gradient tensor, as proposed by Jeong and Hussain[8]. This scalar quantity can be thought of as the total vorticity minus the strain in the flowfield and it enhances the visualization of the rotational tip vortices. These vortices persist for approximately one rotor revolution, which is similar to what was seen in the isolated rotor computations. In addition, the figure shows the interactions between the vortices in the rotor overlap region. Although not apparent from the still image in Figure 5, animations of these results show that each rotor creates a visible pressure pulse as it passes over the

fuselage. The computations provide a wealth of data on the details of the rotor, wake and fuselage interactions.

Figure 6 provides good evidence of this agreement between experimental and computational performance predictions. In this figure, the power predictions give an excellent match to the flight test values over a wide range of vehicle gross weights. The predicted power for all three cases is within a couple of percent of the flight-test values. In addition, Figure 7 shows an excellent correlation between the computational and flight-test figures of merit.

Figure 8 shows a final comparison between legacy empirical and computational results for fuselage download. It compares the computed download fractions to what was estimated empirically. The download fraction is defined as the ratio of the fuselage download to the gross weight of the vehicle. The computational results are remarkably close to the empirical values in that the computed download is within about 13% of the empirical download for all values of gross weight.

The validation is limited to several integrated quantities. The worst situation would be to fortuitously achieve good correlation due to cancellation of different error sources. The next phase of the CFD program will examine the individual component contributions to the integrated thrust and power quantities. Empirical data exist that can help to asses the accuracy of the computed fuselage pressures and the computed induced velocities through the rotor overlap region.

7. Summary and Conclusions

This paper presents computational hover results for the CH-47 Chinook helicopter. The comparison of predicted performance for the installed rotor cases produced excellent agreement with flight test data. The validation is limited in scope to several integrated quantities, but will be expanded upon during future research.

Although the high computational cost for the CFD analysis precludes its use as a general helicopter design tool, the CFD results are quite useful because they provide a huge amount of flowfield detail on rotor-rotor, rotor-wake, and fuselage-wake interactions and this detail can't be obtained in any other way. Details from these complex flowfield interactions may help to suggest design changes that can then be evaluated with flight tests and less computationally-demanding rotorcraft comprehensive analyses.

As mentioned above, all of the calculations in this paper suffer from the fact that they do not include the rotor aeroelastic deflections. Future computational simulations for the CH-47 will include this structural-dynamics and fluid-dynamic modeling for both hover and forward flight cases.

Acknowledgements

This work was funded by the High Performance Computing Modernization Program (HPCMP) under Common High Performance Computing Software Support Initiative Portfolio CST-05, and by the US Army Research, Development, and Engineering Command through contract NNA05BF35C to ELORET. This work was also supported by computer time from the DoD HPCMP at the Naval Oceanographic Office Major Shared Resource Center

References

1. Potsdam, M.A. and R.C Strawn,"CFD Simulations of Tiltrotor Configurations in Hover." *Journal of the American Helicopter Society*, Vol. 50, No. 1, pp. 82–94, Jan. 2005.

2. Khier, W., T. Schwarz, and J. Raddatz, "Time-Accurate Simulation of the Flow around the Complete BO105 Wind Tunnel Model." Presented at the *31st European Rotorcraft Forum*, Florence, Italy, pp. 87.1–87.11, 13–16 Sept. 2005.

3. Pahlke, K., M. Costes, A. D'Alascio, C. Castellin, and A. Altmikus, "Overview of Results Obtained During the 6-Year French-German Chance Project." Presented at the *31st European Rotorcraft Forum*, Florence, Italy, pp. 69.1–69.15, 13–16 Sept. 2005.

4. Stepniewski, W.Z. and C. N.Keys, *Rotary-Wing Aerodynamics*, Dover Publications, Inc., New York, 1984.

Buning, P., G., Gomez, R.J., and W.I. Scallion, "CFD Approaches for Simulation of Wing-Body Stage Separation." *AIAA 2004-4838*, 22nd AIAA Applied Aerodynamics Conference, Providence, RI, August 2004.

5. Chan, W.M., R.L. Meakin, and M.A. Potsdam, "CHSSI Software for Geometrically Complex Unsteady Aerodynamic Applications." *AIAA Paper 2001-0593*, AIAA 39th Aerospace Sciences Meeting and Exhibit, Reno, NV, January 2001.

6. Strawn, R.C., and M.J. Djomehri, "Computational Modeling of Hovering Rotor and Wake Aerodynamics." *AIAA Journal of Aircraft*, Vol. 39, No., pp. 786–7935, Sept. –Oct. 2002.

7. Jeong, J. and F. Hussain, "On the Identification of a Vortex." *Journal of Fluid Mechanics*, Vol. 285, pp. 69–94, 1995.

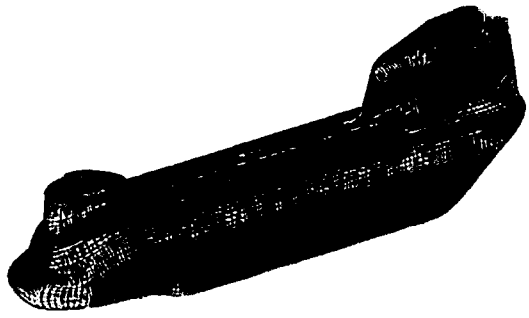

Figure 1. Overset surface grid for CH-47 fuselage

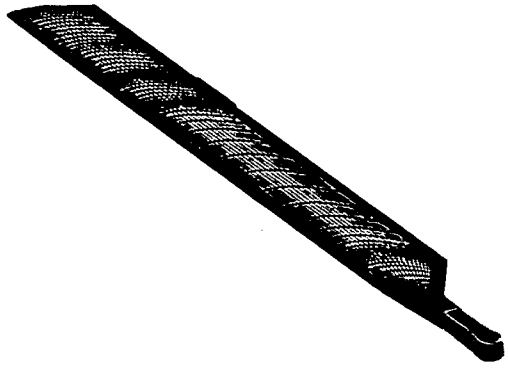

Figure 2. Overset surface grid for one CH-47 rotor blade

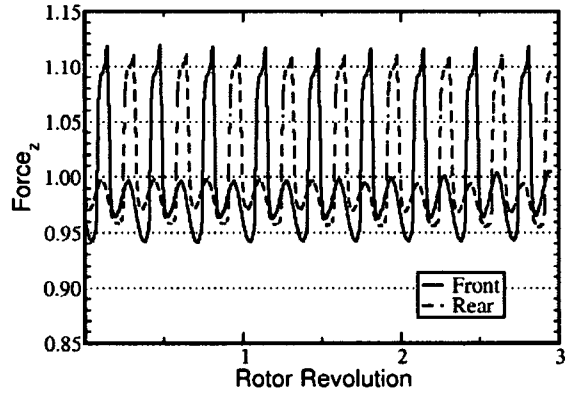

Figure 3. Normalized predictions of rotor thrust for the installed dual rotor CH-47 case at 10° collective angle. (Only the last four rotor revolutions are shown here).

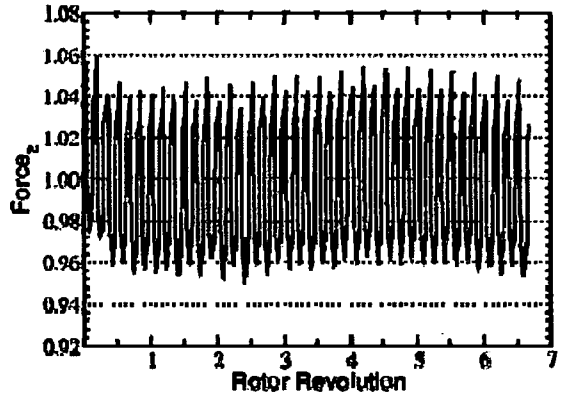

Figure 4. Normalized predictions of total vehicle thrust for the installed dual rotor CH-47 case at 10° collective angle. (Only the last seven rotor revolutions are shown here).

Figure 5. Computed rotor surface pressures and wake geometry for installed dual rotor CH-47 in hover (rotors set at 10° collective angles)

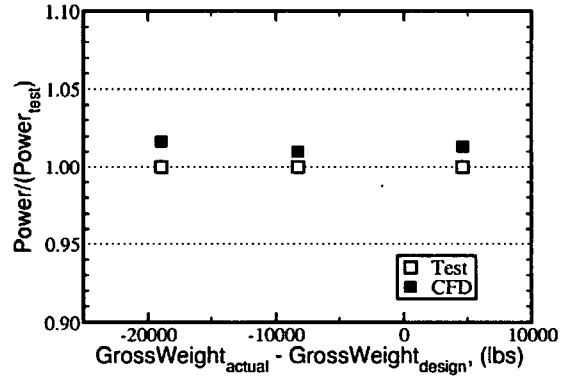

Figure 6. Installed total power and thrust predictions compared to flight test experimental data

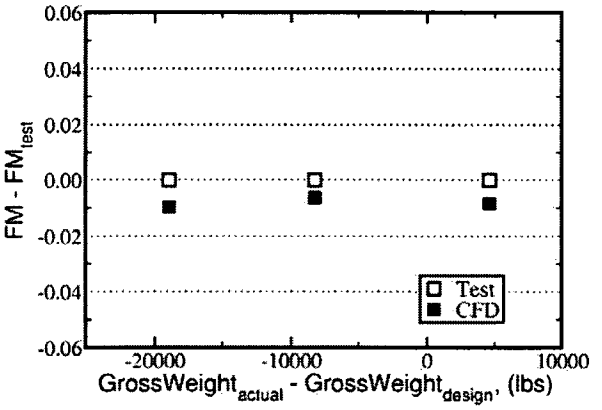

Figure 7. Installed figure of merit (FM) predictions compared to flight test experimental data

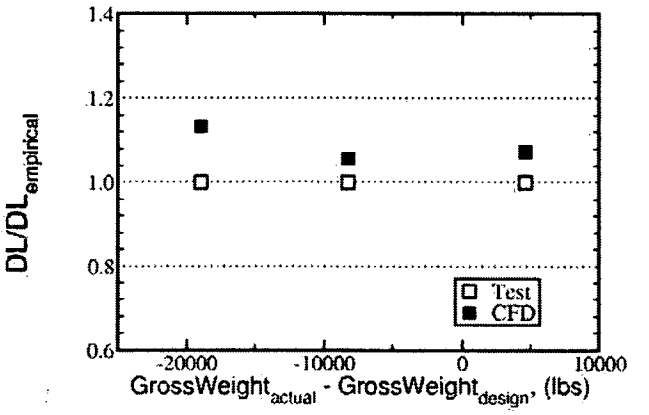

Figure 8. Comparisons between CFD predictions and empirical analysis for rotor fuselage download (DL)